DOI: 10.1002/adma.200601528

High-Modulus Spin-On Organosilicate Glasses for Nanoporous Applications**

By *Hyun Wook Ro*, *Kookheon Char*, *Eun-chae Jeon*, *Hie-Joon Kim*, *Dongil Kwon*, *Hae-Jeong Lee*, *Jin-Kyu Lee*, *Hee-Woo Rhee*, *Christopher L. Soles*,* and *Do Y. Yoon**

Nanoporous glasses, that is, structural glasses with large quantities of nanoscale porosity, are the cornerstone of several emerging technologies. The most prominent example is the semiconductor industry where interlayer dielectric (ILD) insulator films are critically needed to both reduce the resistance–capacitance time delay of the interconnect circuitry and reduce the cross-talk between adjacent conduction lines. For next-generation semiconductors these materials need an ultralow dielectric constant ($k < 2.2$) while being compatible with patterning processes where the minimum features are smaller than 40 nm.[1–6] These structures, owing to their size and dielectric requirements, can only be realized by introducing large quantities of nanoscale porosity. Other technologies where nanoporous glasses are of significant interest include catalyst supports,[7] separations and membranes,[8] laser materials,[9] optical waveguides,[10] sensors,[11] and applications in biotechnology.[12,13]

Adding porosity will generally deteriorate the mechanical properties of a glass, such as the modulus or hardness.[5,6,12] This is especially a problem for the spin-on materials that, even in their nonporous forms, typically have an elastic modulus of less than 5 to 10 GPa.[2,5,12,14] Poly(methylsilsesquioxane) (PMSQ) is perhaps the most common example of a spin-on glass.[2,5,6,12–14] PMSQ organosilicate glasses (OSGs) are attractive for next generation ILD applications because they can be easily spin-cast into smooth films, have inherently low dielectric constants ($k = 2.7$ to 2.9) in their nonporous form, can be rendered porous through the addition of a sacrificial pore generating (porogen) material, and exhibit thermal stability up to 500 °C. However, these materials also tend to be mechanically fragile and inducing porosity significantly worsens the problem. An ILD material must possess the mechanical strength to withstand the harsh and abrasive chemical–mechanical planarization (CMP) processes used in semiconductor fabrication. Higher-modulus materials are superior for withstanding the loads induced by the CMP process. A high elastic modulus is also a desirable property for coating applications in general. Higher-modulus inorganic glass films or coating can be achieved with chemical–vapor deposition (CVD) techniques. However, it is generally realized that spin-on deposition techniques using OSG materials lead to higher-quality films, especially at high porosity. The extendibility of spin-on OSGs to ultralow k films (very high porosity levels) is promising if the modulus of nonporous starting material can be substantially improved. This is the subject of this manuscript.

Another critical property is a low coefficient of thermal expansion (CTE) because of the large temperature changes that are encountered during integration and packaging: a low CTE minimizes the thermal mismatch stresses between the ILD and the other metal or silicon-based materials in the complementary metal oxide semiconductor (CMOS) circuitry that have inherently low CTEs.[1] Most OSGs exhibit CTEs in the range of 100 to 300×10^{-6} °C^{-1}, which is about two orders of magnitude greater than the other "hard" materials found in a CMOS device. The resulting thermal mismatch stresses incurred during integration can lead to catastrophic failure. These liabilities in both the mechanical and thermal properties have precluded the integration of nanoporous materials into state of the art semiconductor devices. There is a pressing need to characterize why these types of nanoporous glasses are so fragile and identify opportunities to increase their thermal and mechanical properties.[15,16]

Our approach is to incorporate organic bridging units into the molecular architecture of PMSQ. PMSQ is typically synthesized through the hydrolytic condensation of methyltrichlorisilane or methyltrimethoxysilane (MTMS—shown in

[*] Dr. C. L. Soles, Dr. H. W. Ro, Dr. H.-J. Lee
Polymers Division, National Institute of Standards & Technology
Gaithersburg, MD 20899 (USA)
E-mail: csoles@nist.gov
Prof. D. Y. Yoon, Dr. H. W. Ro, Prof. H.-J. Kim, Prof. J.-K. Lee
Department of Chemistry, Seoul National University
Seoul 151-747 (Korea)
E-mail: dyyoon@snu.ac.kr
Prof. K. Char
School of Chemical & Biological Engineering
Seoul National University
Seoul 151-742 (Korea)
Dr. E.-c. Jeon, Prof. D. Kwon
School of Materials Science & Engineering
Seoul National University
Seoul 151-747 (Korea)
Prof. H.-W. Rhee
Department of Chemical Engineering, Sogang University
Seoul 121-742 (Korea)

[**] This official contribution of the National Institute of Standards and Technology is not subject to copyright in the United States of America. This work was supported in part by the System IC 2010 Project of Korea, the Chemistry and Molecular Engineering Program of the Brain Korea 21 Project, and the NIST Office of Microelectronics Programs. The authors thank Dr. Robert Cook and Jack Douglas for their careful critique of the manuscript. Supporting Information is available online from Wiley InterScience or from the author.

ADVANCED MATERIALS

the inset of Fig. 1a). The three methoxy groups on each Si atom condense under acidic or basic conditions to form a crosslinked network, with one terminal (noncrosslinked) methyl remaining on each Si. The bridging structure was introduced by blending 1,2-bis(triethoxysilyl)ethane (BTSE—also shown in the inset of Fig. 1a) with the MTMS monomer to create a series of MTMS–BTSE copolymers (see Supporting Information). The BTSE monomer is similar to MTMS in that each Si contains three crosslinkable moieties. The difference is that the terminal methyl of the MTMS is replaced with an ethylene bridge directly connected to a symmetric Si atom, also containing three reactive ethoxy groups. The effect of mixing BTSE with MTMS is to increase the average number of crosslink junctions per monomer. However, the microstructural impact is far more complicated than a simple increase in crosslink density, as elucidated below.

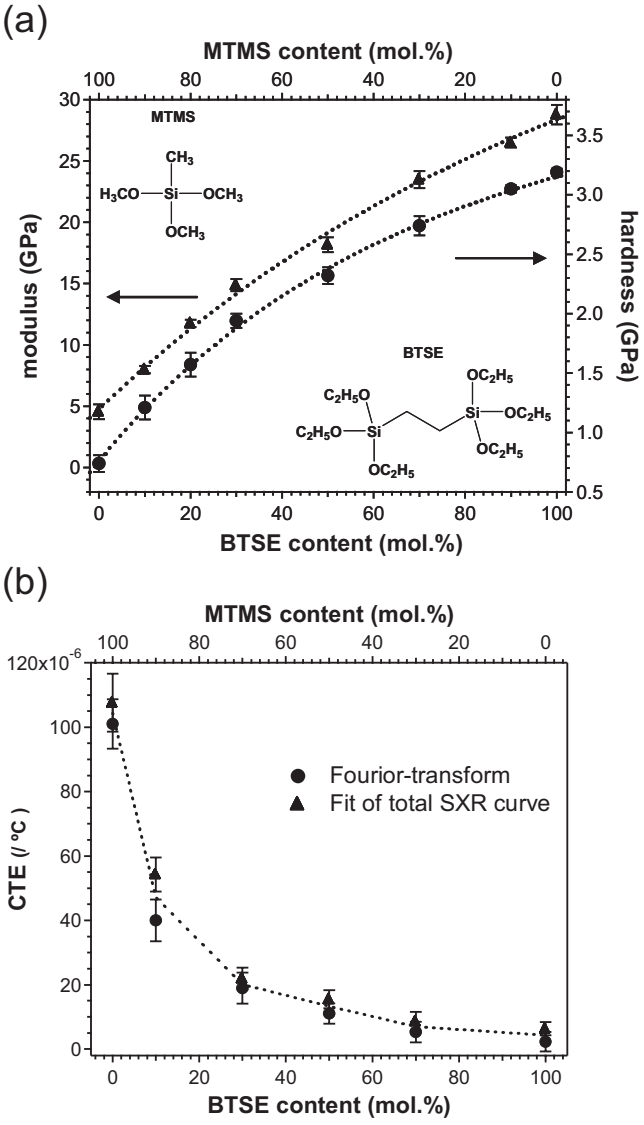

Figure 1. a) The modulus (E_r) and hardness (H) of the films, as characterized by nanoindentation, show a marked increase with the BTSE content. These data are reported when the indentation probe reached a penetration depth 5% of the total film thickness of ca. 1 μm to avoid substrate effects. The arrows indicate the dataset each axis refers to. b) A concomitant decrease in the coefficient of thermal expansion (CTE) with increasing BTSE content was observed with specular X-ray reflectivity.

Nanoindentation measurements quantified the mechanical properties of the MTMS–BTSE copolymer films. Figure 1a shows the apparent Young's modulus and hardness variations with the BTSE composition of the copolymer films. The elastic modulus increased dramatically with BTSE content, from (4.5 ± 0.3) GPa (the error bars presented throughout this manuscript indicate the relative standard uncertainty of the measurement) for the PMSQ homopolymer to (28.8 ± 0.6) GPa for BTSE homopolymer. For spin-on glasses, this increase in modulus is significant. High-modulus ILD materials are superior for withstanding the harsh compressive and shear loads associated with the CMP process. Likewise, Figure 1a shows an equally impressive increase in hardness from (0.75 ± 0.04) GPa for pure PMSQ to (3.20 ± 0.08) GPa in pure BTSE, also quantified by the nanoindentation measurements. High-modulus material can also be brittle, but hardness is more directly related to the yield behavior of the material. The combined observations of a 540% increase in modulus and a 327% improvement in hardness indicate that these materials will be superior for withstanding the harsh CMP process.

It is equally critical to minimize the CTE of an ILD material. The CTEs of the copolymer films were determined from specular X-ray reflectivity (SXR) measurements as a function of temperature,[17,18] either by fitting the complete density profile of the film as a function of thickness, or by simply Fourier transforming the periodicity of the interference fringes in the reflectivity data. The thermal expansion from 25 to 175 °C is linear and the CTE was derived from the slope of the fit normalized by the total film thickness at 25 °C. Figure 1b shows that for both methods the CTE decreases exponentially with the BTSE content. A small amount of BTSE is very effective at reducing the large CTE of PMSQ.

The use of BTSE to improve the critical mechanical and thermal properties of the PMSQ homopolymer is, however, accompanied by an increase in the dielectric constant and the refractive index as shown in Table 1. The Clausius–Mossotti equation indicates that the increase in k can be related to either an increase in the index of refraction or an increase of density. From Table 1 the index of refraction varies slightly with the organic bridging, but the affect the BTSE had on the density remained to be seen. Therefore, X-ray porosimetry (XRP) measurements were used to quantify the density and intrinsic porosity of the MTMS–BTSE copolymer films. The intrinsic porosity is the native porosity of the resin before the porogen is added. XRP combines SXR with the mechanism of capillary condensation.[19–21] SXR measurements of the copolymer film in vacuo determined the average film density $\rho_{average}$: an average that includes contributions from the intrinsic porosity. In the presence of a saturated organic vapor, such as methyl ethyl ketone (MEK), capillary condensation

Table 1. Physical properties of the organosilicate films as determined by using X-ray porosimetry (XRP), ellipsometry, and capacitance measurements. ρ_{dry} is the average density in vacuum and ρ_{wall} is wall density of the material between the intrinsic pores.

Composition BTSE [mol %]	ρ_{dry} [g cm^{-3}]	XRP ρ_{wall} [g cm^{-3}]	Porosity [%]	k (1 MHz)	Rrefractive index (632.8 nm)
0	1.221 ± 0.005	1.303 ± 0.005	6.7 ± 1.0	2.75 ± 0.03	1.38 ± 0.05
10	1.285 ± 0.005	1.355 ± 0.005	5.2 ± 1.0	2.81 ± 0.06	1.39 ± 0.07
30	1.359 ± 0.005	1.456 ± 0.005	6.7 ± 1.0	2.92 ± 0.08	1.40 ± 0.03
50	1.418 ± 0.005	1.518 ± 0.005	6.6 ± 1.0	3.02 ± 0.05	1.41 ± 0.11
70	1.497 ± 0.005	1.517 ± 0.005	1.3 ± 1.0	3.14 ± 0.05	1.42 ± 0.08
90	1.523 ± 0.005	1.552 ± 0.005	1.9 ± 1.0	–	1.47 ± 0.05
100	1.582 ± 0.005	1.604 ± 0.005	1.3 ± 1.0	–	1.48 ± 0.10

occurs in the nanoporous cavities of the film, increasing the density of the film. SXR measurements in the presence of the vapor revealed the saturated film density $\rho_{saturated}$. The porosity P and wall density of the material between the intrinsic pores ρ_{wall} were determined by simultaneously solving the following equations, taking $\rho_{solvent}$ to be the bulk density of the liquid solvent condensed inside the pores:

$$\rho_{average} = \rho_{wall} \times (1 - P) \quad (1)$$

$$\rho_{saturated} = \rho_{solvent} \times P + \rho_{wall} \times (1 - P) \quad (2)$$

Table 1 shows that both $\rho_{average}$ and ρ_{wall} increased with the amount of BTSE. The intrinsic porosity of the PMSQ homopolymer is (6.7 ± 1) % by volume and it did not vary significantly with the addition of approximately 50 mol % BTSE. Beyond 50 mol % BTSE, a step-like decrease in the porosity appeared that is correlated with a step-like discontinuity in the dependence of ρ_{wall} on the BTSE content. Notice that the $\rho_{average}$ did not exhibit a similar discontinuity. BTSE increased the crosslink density of the PMSQ so it is reasonable to anticipate more efficient atomic and/or molecular packing, that is, a reduction of the unoccupied volume. However, the ability of XRP to probe this unoccupied volume is predicated on filling the volume with MEK. Pores that become too small may be inaccessible for the probe solvent molecules. As will be discussed later, the addition of BTSE promotes the formation of small cage and cyclic microstructures that have interior regions that are inaccessible by MEK or other organic solvent molecules. The apparent discontinuity in the evolution of ρ_{wall} and P at high BTSE content probably reflects the formation of such inaccessible pores. Nevertheless, the increased apparent modulus and hardness in Figure 1a can be ascribed to the increases in the average film and wall densities.

It is generally understood that density and the CTE are anticorrelated. A subtle, but important, distinction is that BTSE increases both the extent of network formation (degree of crosslinking) and the density. However, increased crosslinking alone may not be sufficient to rationalize the reduced CTE of the glassy film. Studies on epoxy networks where the crosslink density was significantly varied but the density remained, to a first approximation, constant did not produce noticeable variations in the glassy-state CTEs.[22] In this respect, the reduced CTE here most likely reflects the increased density, not the increased crosslinking.

The preceding discussion described how the addition of the BTSE co-monomer greatly enhanced the mechanical and thermal properties the OSGs. The molecular origins of these enhancements are now discussed. The hydrolytic condensation of alkyl trifunctional silanes, such as MTMS, propyltrimethoxysilane (PTMS), or isobutyl trimethoxysilane (i-BTMS), can lead to the formation of both loosely branched networks as well as intramolecular cyclic silsesquioxanes (SSQs), including the perfect (i.e., completely closed) T_8, T_{10}, T_{14}, and T_{16} cage structures.[23] The tendency to form cyclic or cage-type SSQs increases with the size of organic substituent, owing to steric hindrances.[23] In the PMSQ homopolymer the tendency to form open-branched microstructures is slightly favored in the initial stages of the reaction,[24] but the intramolecular cyclization and intermolecular chain-extension reactions become competitive in the later stages of conversion. This leads to a mixture of both perfect and partial cage structures with a crosslinked or ladder-like network. It is critical to realize that the vertices or corners of a perfect cage are terminated with nonreactive methyl groups; these perfect cage structures, once formed, cannot be covalently attached to the rest of the network. As we show below, they are in many ways incompatible with the network structure in films.

To spin-cast a smooth OSG film, the monomers were partially condensed in an acidic solution to produce an oligomeric or polymeric product. This product was collected and redissolved into an organic solvent suitable for spin-coating. The spin-cast film was then condensed into a hard glassy network structure at 430 °C under an inert atmosphere. For pure PMSQ, the initial reaction products included both a white precipitate that dropped out of the acidic solution, as well as an aqueous gel. Fourier transform infrared (FTIR) spectroscopy confirmed that the precipitate consisted primarily of the octamethyl-T_8 perfect cage structure (Supporting Information, Fig. S1).[25] The remaining soluble reaction products in the gel were characterized by graphite-plate laser-desorption/ionization mass spectrometry (GPLDI-TOF MS) (Fig. 2a). The major reaction product below 1000 Da (1 Da ~ 1.66×10^{-27} kg) for the PMSQ homopolymer consisted of incomplete cage-type microstructures possessing two or three silanol groups such as the $T_7(OH)_3$ (m/z 520.8 ($+Na^+$) and 537.9 ($+K^+$)), $T_8(OH)_2$ (m/z 577.3 ($+Na^+$) and 595.5 ($+K^+$)), $T_9(OH)_3$ (m/z 653.1 ($+Na^+$) and 669.9 ($+K^+$)), and $T_{10}(OH)_2$ (m/z 712.7 ($+Na^+$) and 728.8 ($+K^+$)), consistent with the propensity to form cyclics in the early stages of conversion. The perfect cage structures, such as octamethyl-T_8, are not seen in the GPLDI-TOF MS because they lack the silanol

ADVANCED MATERIALS

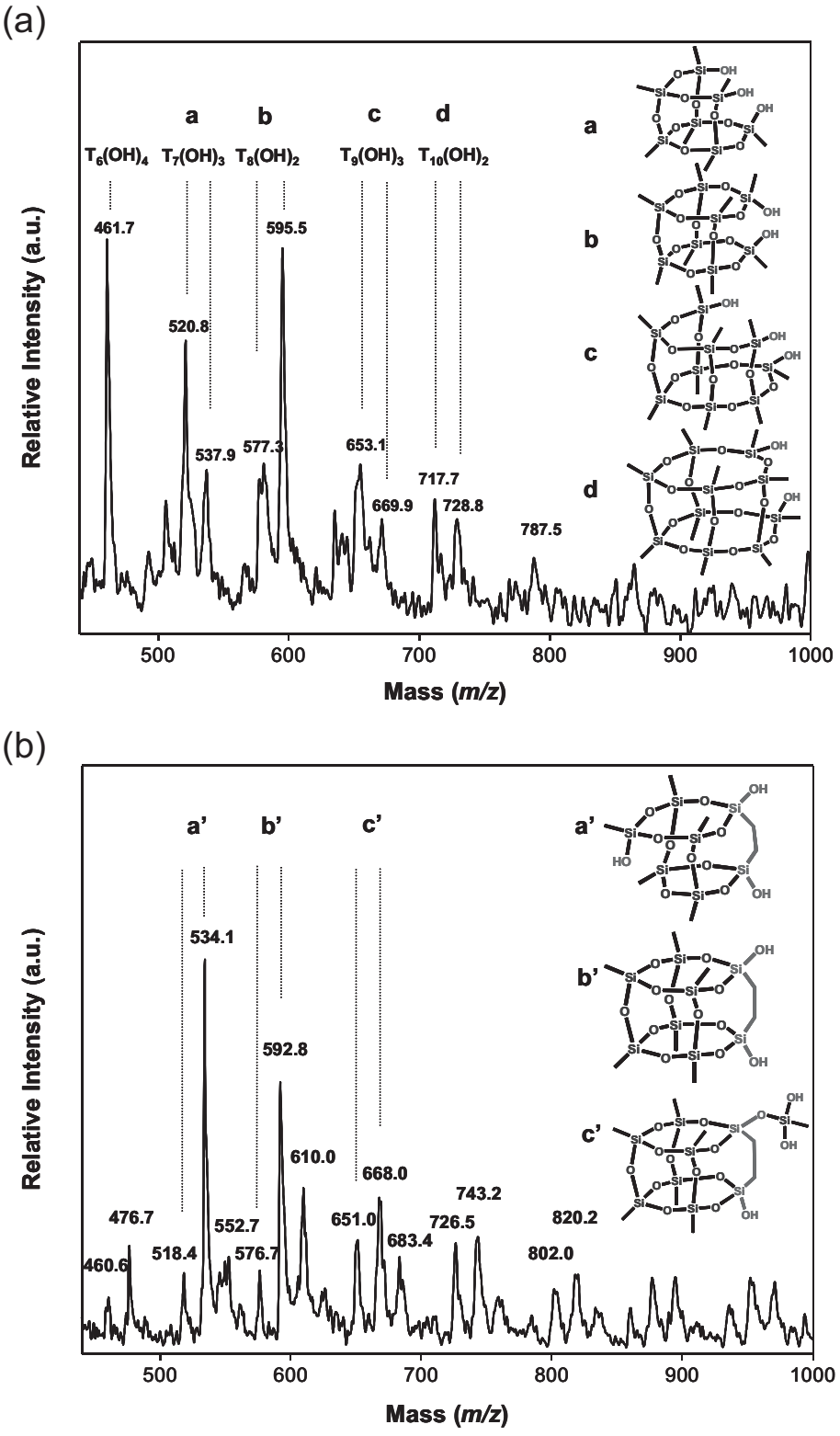

Figure 2. The GPLDI-TOF MS spectra are shown for a) the PMSQ (MTMS) homopolymer and b) the MTMS/BTSE (9:1) copolymer sol–gel reaction products. The incorporation of the BTSE monomer promotes the formation of closed-cage microstructures with the silanol functionality that is needed to later covalently attach the cage to the crosslinked network when the spin-cast film is fully converted into an organosilicate at elevated temperature.

functionality and therefore precipitated out of solution. These partial-cage structures comprised of 7 to 12 Si atoms are quite stable and do not typically grow by chain-extension reactions in the latter stages of conversion while the network structures are forming.

The isolated perfect- or partial-cage structures are important for understanding the poor mechanical properties of the PMSQ films. The open and branched SSQ networks have a large silanol content, whereas the closed cage-type SSQs, especially the perfect cages, contain very few silanols. For this reason there is a propensity for aggregation or phase separation of cage-type SSQs from the silanol-rich network.[26–28] The as-cast films fabricated from PMSQs containing cage-type species were initially transparent and defect free. Upon heating to 100 °C, these films became partially opaque, turning highly opaque with many defects after full conversion at 430 °C. Defects that scatter light were created upon heating. It is worth mentioning that the PMSQ reaction conditions could be manipulated to yield a larger fraction of small cage-type species, which then led to a film with more defects upon vitrification. X-ray diffraction measurements on the transparent as-cast films revealed crystalline peaks, suggesting phase-separated domains of the crystallized cage structures (Supporting Information Fig. S2). These crystalline peaks disappeared when the film was heated beyond 300 °C, suggesting that the phase-separated perfect cages sublimed or evaporated. Thermal gravimetric analysis confirmed this mass loss. This is reasonable given that perfect cages are not covalently attached to the network and that the pure T_8 compound sublimes above 200 °C. The loss of these phase-separated crystalline MSQ domains left behind large porous defects that scattered light, and more importantly, contrib-

uted to the low modulus and poor hardness of the PMSQ homopolymer film.

Adding small amounts of the BTSE co-monomer to the PMSQ prohibited the formation of the insoluble and isolated cage structures. The first evidence for this was the absence of the precipitates in the acidic reaction mixture. The GPLDI-TOF MS of the MTMS–BTSE (9:1) copolymer in Figure 2b indicated small cage-type fragments such as the $T_7(OH)_3$ (m/z 517.8 ($+Na^+$) and 533.9($+K^+$)) and $T_8(OH)_2$ (m/z 575.9 ($+Na^+$) and 592.0 ($+K^+$)) structures in the molecular mass region below 1000 Da. This confirmed that the BTSE monomer could be successfully incorporated into the perfect-cage structures. It is crucial to realize that the perfect or closed-cage structures containing the BTSE monomer retained their silanol functionality. This is unlike the PMSQ material where the closed-cage structures contained only nonreactive methyl groups. The silanol functionality promoted solubility in the acidic reaction solution and the perfect cages did not precipitate out of the reaction mixture. Crystalline X-ray diffraction peaks were no longer observed in the as-cast film containing BTSE. Moreover, the silanols were able to react during the final conversion and could be covalently incorporated into the growing network.

We found that adding BTSE increased the population of the functionalized small-cage structures in both the sol–gel reaction products and the final film. The retention of these small-cage structures was the primary reason for vastly improved modulus, hardness, and CTE values of the copolymers films. This could be shown through solution-state ^{29}Si NMR measurements on the sol–gel reaction products that were collected and spin-cast into the initial films. Figure 3 shows three characteristic peaks in the PMSQ spectrum denoted T^3, T^2, and T^1. These peaks reflect Si bonded to three O atoms through Si–O–Si bonds (T^3), Si bonded to two O atoms through Si–O–Si bonds and one terminal OH group (T^2), or Si bonded to one O atom through Si–O–Si bonds and two terminal OH groups (T^1). The T^3, T^2, and T^1 peaks are sensitive to the bond angles associated with Si. A discrete downfield shift occurred in each of the characteristic peaks when the Si was strained into a small cyclic structure. Loy et al. used this downfield shift to characterize the acid-catalyzed SSQ sol–gel reaction products and found that ethylene-, propylene-, and butylene-bridged alkoxysilanes have a strong tendency to form such cyclic structures.[29] In Figure 3 the T^1, T^2, and T^3 peaks were seen near –47 ppm, –57 ppm, and <M>65 ppm, respectively, with no T^1 peak observed in the PMSQ homopolymer. As the BTSE loading increased, new peaks emerged near –52 ppm and –60 ppm, identified as cyclic variations of the T^2 and T^3 peaks, respectively.[29] Increasing the BTSE loading increased the fraction of the small cyclic structures in the initial reaction products that were spin-cast into the films. Transmission FTIR spectra of the copolymer films both as-cast and after the final conversion at 430 °C supported the conclusions from the NMR analysis (Supporting Information Fig. S3). Like the NMR spectra, the characteristic peaks in the FTIR spectra of cyclized alkoxysilanes

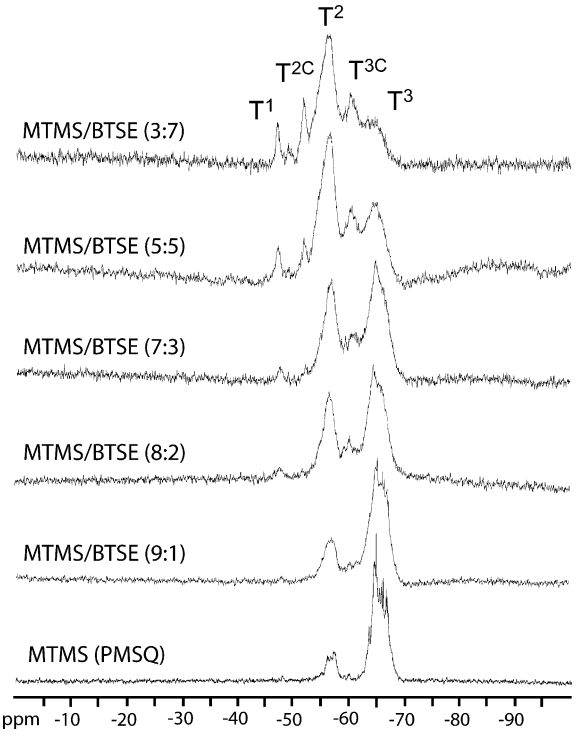

Figure 3. The solution state ^{29}Si NMR data are shown for the sol–gel reaction products prior to spin-coating the OSG films. There are three characteristic peaks in the pure PMSQ spectrum denoted T^3, T^2, and T^1. A discrete downfield shift occurs in the T^3 and T^2 peaks when BTSE is added to the reaction mixture, producing peaks T^{3c} and T^{2c}. As described in the text, this indicates that the addition of BTSE promotes the formation of small strained cyclic OSG structures.

generally shifted to lower frequencies in comparison to their noncyclized analogs.[30] The as-cast films of the pure PMSQ exhibited characteristic Si–O–Si and Si–OH peaks of both the perfect cages and the branched-type microstructures. After full conversion the strained cyclic peaks decreased significantly in intensity and the branched network structures became dominant. On the contrary, for high BTSE loadings the strained cyclic structures were dominate both in the as-cast and the fully converted films.

In addition to the modulus and CTE improvements, the increased silanol content can have the added benefit of increasing the miscibility of the porogen with the matrix material. A detailed discussion of how adding porosity impacts the physical properties is beyond the scope of this communication, which is dedicated, instead, to improving the matrix materials themselves. However, it is generally realized that many porogen systems are based on diblock or triblock copolymers where one of the blocks is hydrophilic to promote solubility with the silanol-containing as-cast film, whereas the others are hydrophobic to promote phase separation. The result is phase separation on very small length scales and thus small pores. By increasing the silanol content one can increase the effective solubility of the porogen in the matrix. Preliminary experiments on these systems, even with just a moderate

ADVANCED MATERIALS

BTSE content, showed that they could be loaded with as much as 50 % by mass of the common Textronic porogen (a PEO–PPO–PEO block copolymer; PEO = poly(ethylene oxide), PPO = poly(propylene oxide)) and were successfully vitrified without degrading the film quality. This extendibility to high porosities is one of the strengths of the spin-on OSG systems over current CVD technologies. How this porosity affects the physical properties will be the subject of an ensuing article.

We now better understand why the PMSQ type organosilicates exhibit poor thermal and mechanical properties. This is primarily because the PMSQ monomers form a breadth of microstructures in the initial stages of the reaction, including open networks, partial cages with relatively large cyclic structure, as well as some of the small strained cyclics such as the perfect T_8 cage. The larger and inherently more flexible Si–O–Si bond architectures generally contribute to the low modulus and large CTE of PMSQ. The problem is exacerbated during the high-temperature vitrification where the small strained perfect cages are lost by evaporation or sublimation. This reduces the density and leaves behind porous defects in the final film. The addition of BTSE to the reaction mixture biases the microstructure yield towards smaller cages and strained cyclics with more rigid Si–O–Si bond architectures. More importantly, these small-cage structures, even the perfect cages, retain the critical silanol functionality. The silanols prevent phase separation and allow the perfect cages to be covalently incorporated into the crosslinked network. The result is a moderately denser film with vastly improved modulus, hardness, and CTE values. This means there will be a trade-off developing ultralow *k* materials. The improved thermal and mechanical properties must be balanced against the effective increase in *k*. It should also be realized that the extrinsic porosity has not yet been added to these materials. Inducing porosity through addition of a porogen can easily offset the small increase in *k* of the wall material.

Received: July 7, 2006
Revised: September 25, 2006
Published online: February 1, 2007

[1] The International Technology Roadmap for Semiconductors: 2005, Semiconductor Industry Association, http://www.itrs.net/Links/2005ITRS/Home2005.htm (accessed January 2007).
[2] C. V. Nguyen, K. R. Carter, C. J. Hawker, J. L. Hedrick, R. L. Jaffe, R. D. Miller, J. F. Remenar, H.-W. Rhee, P. M. Rice, M. F. Toney, M. Trollsas, D. Y. Yoon, *Chem. Mater.* **1999**, *11*, 3080.
[3] K. Landskron, B. D. Hatton, G. A. Ozin, *Science* **2003**, *302*, 266.
[4] R. A. Pai, R. Humayun, M. T. Schulberg, A. Sengupta, J.-N. Sun, J. J. Watkins, *Science* **2004**, *303*, 507.
[5] S. Yang, P. Mirau, C. S. Pai, O. Nalamasu, E. Reichmanis, J. C. Pai, S. Y. Obeng, J. Seputro, E. K. Lin, H.-J. Lee, J. Sun, D. W. Gidley, *Chem. Mater.* **2002**, *14*, 369.
[6] H. W. Ro, K. J. Kim, P. Theato, D. W. Gidley, D. Y. Yoon, *Macromolecules* **2005**, *38*, 1031.
[7] J. L. Defreese, A. Katz, *Chem. Mater.* **2005**, *17*, 6503.
[8] H. Dong, M. A. Brook, J. D. Brennan, *Chem. Mater.* **2005**, *17*, 2807.
[9] P. Yang, G. Wirnsberger, H. C. Huang, S. R. Cordero, M. D. McGehee, B. Scott, T. Deng, G. M. Whitesides, B. F. Chmelka, S. K. Buratto, G. D. Stucky, *Science* **2000**, *287*, 465.
[10] W.-C. Chen, L.-H. Lee, B.-F. Chen, C.-T. Yen, *J. Mater. Chem.* **2002**, *12*, 3644.
[11] B. J. Scott, G. Wirnsberger, G. D. Stucky, *Chem. Mater.* **2001**, *13*, 3140.
[12] H.-C. Kim, G. Wallraff, C. R. Kreller, S. Angelos, V. Y. Lee, W. Volksen, R. D. Miller, *Nano Lett.* **2004**, *4*, 1169.
[13] H.-C. Kim, C. R. Kreller, K. A. Tran, V. Sisodiya, S. Angelos, G. Wallraff, S. Swanson, R. D. Miller, *Chem. Mater.* **2004**, *16*, 4267.
[14] R. F. Cook, E. G. Liniger, *J. Electrochem. Soc.* **1999**, *146*, 4439.
[15] E. P. Guyer, R. H. Dauskardt, *Nat. Mater.* **2004**, *3*, 53.
[16] D. A. Maidenberg, W. Volksen, R. D. Miller, R. H. Dauskardt, *Nat. Mater.* **2004**, *3*, 464.
[17] C. E. Bouldin, W. E. Wallace, G. W. Lynn, S. C. Roth, W. L. Wu, *J. Appl. Phys.* **2000**, *88*, 691.
[18] W.-L. Wu, H.-C. Liou, *Thin Solid Films* **1998**, *312*, 73.
[19] W.-L. Wu, W. E. Wallace, E. K. Lin, G. W. Lynn, C. J. Glinka, E. T. Ryan, H.-M. Ho, *J. Appl. Phys.* **2000**, *87*, 1193.
[20] H. J. Lee, C. L. Soles, D. W. Liu, B. J. Bauer, W. L. Wu, *J. Polym. Sci. Part B* **2002**, *40*, 2170.
[21] H. J. Lee, C. L. Soles, D. W. Liu, B. J. Bauer, E. K. Lin, W. L. Wu, A. Grill, *J. Appl. Phys.* **2004**, *95*, 2355.
[22] C. L. Soles, *Ph.D. Thesis*, University of Michigan **1998**.
[23] H.-J. Kim, J.-K. Lee, J. B. Kim, E. S. Park, S. J. Park, D. Y. Yoo, D. Y. Yoon, *J. Am. Chem. Soc.* **2001**, *123*, 12 121.
[24] H.-J. Kim, J.-K. Lee, S.-J. Park, H. W. Ro, D. Y. Yoo, D. Y. Yoon, *Anal. Chem.* **2000**, *72*, 5673.
[25] L.-H. Lee, W.-C. Chen, W.-C. Liu, *J. Polym. Sci. Part A* **2002**, *40*, 1560.
[26] L. Zheng, A. J. Waddon, R. J. Farris, E. B. Coughlin, *Macromolecules* **2002**, *35*, 2375.
[27] G.-M. Kim, H. Qin, X. Fang, F. C. Sun, P. T. Mather, *J. Polym. Sci. Part B* **2003**, *41*, 3299.
[28] A. Strachota, I. Kroutilova, J. Kovarova, L. Matejka, *Macromolecules* **2004**, *37*, 9457.
[29] D. A. Loy, J. P. Carpenter, T. M. Alam, R. Shaltout, P. T. Dorhout, J. Greaves, J. H. Small, K. J. Shea, *J. Am. Chem. Soc.* **1999**, *121*, 5413.
[30] W. Norman, J. H. Melvin, *J. Am. Chem. Soc.* **1947**, *69*, 803.

